J. Radiat. Res., 51, 633–641 (2010)

Regular Paper

Early Increase of Radiation-induced γH2AX Foci in a Human Ku70/80 Knockdown Cell Line Characterized by an Enhanced Radiosensitivity

Veerle VANDERSICKEL[1], Julie DEPUYDT[1], Bram VAN BOCKSTAELE[2], Gianpaolo PERLETTI[3], Jan PHILIPPE[4], Hubert THIERENS[1] and Anne VRAL[1]*

H2AX phosphorylation/Ionizing radiation/DNA double strand breaks/Ku70/80 heterodimer/Radiosensitivity.

A better understanding of the underlying mechanisms of DNA repair after exposure to ionizing radiation represents a research priority aimed at improving the outcome of clinical radiotherapy. Because of the close association with DNA double strand break (DSB) repair, phosphorylation of the histone H2AX protein (γH2AX), quantified by immunodetection, has recently been used as a method to study DSB induction and repair at low and clinically relevant radiation doses. However, the lack of consistency in literature points to the need to further validate the role of H2AX phosphorylation in DSB repair and the use of this technique to determine intrinsic radiosensitivity. In the present study we used human mammary epithelial MCF10A cells, characterized by a radiosensitive phenotype due to reduced levels of the Ku70 and Ku80 repair proteins, and investigated whether this repair-deficient cell line displays differences in the phosphorylation pattern of H2AX protein compared to repair-proficient MCF10A cells. This was established by measuring formation and disappearance of γH2AX foci after irradiating synchronized cell populations with ^{60}Co γ-rays. Our results show statistically significant differences in the number of γH2AX foci between the repair-deficient and -proficient cell line, with a higher amount of γH2AX foci present at early times post-irradiation in the Ku-deficient cell line. However, the disappearance of those differences at later post-irradiation times questions the use of this assay to determine intrinsic radiosensitivity, especially in a clinical setting.

INTRODUCTION

DNA double strand breaks (DSBs) are one of the most genotoxic lesions in the genome generated by endogenous or exogenous agents such as ionizing radiation. If not repaired or misrepaired they can result in the disruption of the genomic integrity through the formation of chromosome aberrations, which can lead to carcinogenesis.[1)] Because of the importance of correct DNA DSB repair, eukaryotic cells respond to DSBs by activating complex and highly conserved systems to rapidly and efficiently detect DSBs, signal their presence and execute repair.[2)] Two distinct pathways that mediate DSB repair have been identified in mammalian cells: Homologous Recombination and Non-Homologous Endjoining (NHEJ). The more error prone NHEJ is the main pathway to repair radiation-induced DSBs. One of the key players of this pathway is the Ku70/80 heterodimer. This dimer, which consists of a 70 and 86 kDa protein, Ku70 and Ku80 respectively, binds to the broken DNA ends with high affinity and then recruits the catalytic subunit of the DNA-dependent protein kinase (DNA PKcs). Activated DNA PKcs will in turn further phosphorylate proteins including itself necessary for efficient processing and finally ligation of the break.[3,4)] The importance of the Ku70 and Ku80 proteins in DNA DSB repair is well illustrated by several reports describing a marked increase in cellular radiosensitivity of both mutant rodent cell lines defective in Ku80

*Corresponding author: Phone: +32(9)332-5129,
Fax: +32(9)332-3823,
E-mail: Anne.vral@UGent.be
[1]Department of Basic Medical Sciences, Ghent University, De Pintelaan 185, 9000 Gent, Belgium; [2]Department of Experimental-Clinical and Health Psychology, Ghent University, Henri Dunantlaan 2, 9000 Gent, Belgium; [3]Department of Structural and Functional Biology, Laboratory of Toxicology and Pharmacology, Università degli Studi dell' Insubria, via A. Da Guissano 10, 21052 Busto Arsizio, Italy; [4]Department of Clinical Biology, Microbiology and Immunology, Ghent University, De Pintelaan 185, 9000 Gent, Belgium.
doi:10.1269/jrr.10033

(e.g., the *xrs*-5 and *xrs*-6 cell line)[5] and human cell lines that have reduced expression levels of the Ku70 or Ku80 proteins.[6–14]

To understand the mechanisms that lead to a radiosensitive phenotype characterized by an enhanced number of chromosome aberrations, the efficiency and kinetics of DSB repair/rejoining are often investigated. For this, physical methods such as neutral sucrose density gradient centrifugation, neutral filter elution, single cell gel electrophoresis (= comet assay) and pulsed field gel electrophoresis (PFGE) are conventionally used. The disadvantage of these assays is that they require high irradiation doses for a reliable assessment of the rejoining kinetics.[15,16] Recently, H2AX phosphorylation, quantified by specific immunodetection, has been described as a valuable and highly sensitive method to monitor DSB induction and repair at lower and clinically more relevant doses.[15–20]

The H2AX protein is a sequence variant of the H2A histone and represents about 2–25% of the total H2A pool in mammalian cells. Together with 3 other highly conserved histone proteins, H2B, H3 and H4, H2A forms the histone octamer. Wrapping of 147 bp of DNA around this octamer gives then rise to the nucleosome, the basic unit of chromatin.[21] In response to radiation-induced DSBs, the serine 139 within the conserved C-terminal region of the H2AX protein becomes phosphorylated[22,23] by one of the DNA damage signaling kinases of the phosphatidylinositol-3-OH-kinase-like (PIKK) family.[24,25] This phosphorylation rapidly spreads to a large chromatin region surrounding the DSB, resulting in the formation of γH2AX foci. These foci are detectable within 3 min after irradiation and their number increases until 10–30 min after irradiation. As a consequence of their ability to attract specific proteins[26] the main role of H2AX phosphorylation in the DNA damage response has been argued to be the recruitment of DNA damage repair proteins to the sites of DSBs and the generation of a platform for signaling and repair (for a review, see Kinner *et al.*[15]). Based on the findings that no other lesion than the DNA DSB induces H2AX phosphorylation and that the number of γH2AX foci is closely related to the number of radiation-induced DNA DSBs,[22,27,28] γH2AX foci formation can be considered as a consistent and quantitative marker of radiation-induced DNA DSBs.[15] However, the relationship between DNA DSB repair and the disappearance of γH2AX foci is less well understood. Due to its function in the DNA damage response, loss of γH2AX has been proposed to reflect DSB repair/rejoining.[28–31] However, several reports describe a disparity between the actual removal of DSBs as measured by physical methods of DSB detection, and the removal of γH2AX foci.[15,32,33] Analysis of DSB rejoining using PFGE in irradiated cells reveals that the kinetics of rejoining DSBs are biphasic and comprise a fast component operating with half times of several min followed by a slow component that rejoins remaining DSBs with a half time of a few hours.[34–38] Considering that γH2AX foci formation increases up to 30 min after irradiation, the loss of γH2AX seems unlikely to coincide with the physical sealing of the DSB.[15] Although the understanding of the role of γH2AX foci in DSB repair is incomplete, several investigators tried to correlate γH2AX disappearance and the residual amount of γH2AX foci remaining at longer times post-irradiation (generally 24 h) with the intrinsic radiosensitivity of a cell line.[33,39–44] Banath *et al.*[39] reported a correlation between residual levels of γH2AX foci 24 h after irradiation and clonogenic survival at a dose of 2 Gy in six human cervical cancer cell lines. Furthermore, Taneja *et al.*[40] observed that radiosensitive tumor cells retained γH2AX foci for a longer duration than radioresistant tumor cell lines (see also MacPhail *et al.*[41]). On the other hand, Mahrhofer *et al.*[42] failed to observe a correlation between cellular radiosensitivity and both the kinetics of disappearance and the residual amounts of γH2AX foci in 10 human tumor and normal cell lines. In addition, Yoshikawa *et al.*[44] found no close correlation between residual γH2AX foci and radiosensitivity in some tumor cell lines, while in normal human cells residual γH2AX foci were closely correlated with lethal sensitivity.

These divergent results point to the need to further validate the role of H2AX phosphorylation in DSB repair and the use of this technique to determine intrinsic radiosensitivity. To date, research reports investigating γH2AX foci induction and loss in Ku70/80 repair-deficient cell lines in detail are restricted to studying Ku defective hamster cell lines (*xrs*-5 and *xrs*-6).[33,45] However, accumulating evidence suggests that the requirement and/or function of the Ku proteins may differ between rodents and humans.[6,10] Therefore, we used human mammary epithelial MCF10A cells that have reduced levels of the Ku70 and the Ku80 proteins, due to RNAi of Ku70. In a previous study,[14] we found that these Ku-defective cells are characterized by an increase in chromosomal and cellular radiosensitivity compared to their Ku-proficient counterpart. In the present study, we examined if the Ku repair-deficient cell line also displays differences in the phosphorylation pattern of H2AX protein compared to the repair proficient MCF10A cells. This was established by measuring induction and kinetics of γH2AX foci disappearance after *in vitro* exposure to ^{60}Co γ-rays.

MATERIALS AND METHODS

Cell lines

MCF10A cells, spontaneously immortalized human breast epithelial cells, were cultured as monolayers in growth medium consisting DMEM/F12-Ham (1:1) supplemented with 10 μg/ml insulin, 0.5 μg/ml hydrocortisone, 20 ng/ml epidermal growth factor, 50 U/ml penicillin and 50 μg/ml streptomycin and 5% horse serum, in a humidified 5% CO_2 incubator at 37°C. To generate a repair-deficient cell line, MCF10A cells were transduced with lentiviral particles har-

boring DNA sequences encoding for short hairpin RNA specific for Ku70 RNA interference (= Ku70i cells). As a control cell line, MCF10A cells were mock-transduced with 'empty' lentiviral particles (= LVTHM cells). More details can be found in Vandersickel *et al*.[14] Protein expression silencing of Ku70 and Ku80 by western blot analysis was evaluated in Ku70i and LVTHM cells. When a stable knockdown was achieved in the Ku70i cells, these cells were used for *in vitro* irradiation experiments.

Synchronization

During the S-phase of the cell cycle endogenous DNA DSBs may arise from the accidental stoppage and collapse of replication forks. To diminish the occurrence of endogenously produced DSBs, cells were synchronized in the G0/G1 phase of the cell cycle, where spontaneous levels of DNA DSBs are generally low.[46,47] Synchronization was established through serum deprivation of exponentially growing Ku70i and LVTHM cells. At day zero, 5×10^6 exponentially growing cells were seeded in T75 culture flasks in normal growth medium. At day one, the growth medium was aspirated and replaced by DMEM/F12-Ham deprived of growth factors and horse serum (= serum starvation medium). Flow cytometric analysis showed that at day two, more than 90% of the cells were in G0/G1 phase of the cell cycle.

Irradiation experiments

Synchronized MCF10A cells (LVTHM and Ku70i) were harvested by trypsinization and resuspended in serum starvation medium at a concentration of 8×10^5 cells/2 ml. For the dose response experiments, 2 ml cultures were irradiated with a dose of 0.2, 0.5, 1, 2, 3 and 4 Gy in a water bath at 37°C with ^{60}Co γ-rays at 0.5 Gy/min. For the repair kinetics experiments, cultures were irradiated with a dose of 1 Gy. Within each experiment, sham-irradiated cell cultures were also included.

After irradiation, cell cultures were further incubated at 37°C to allow foci formation. For the dose response experiments, cultures were stopped 15 min post irradiation by placing the cultures on ice. After 10 min, 0.5 ml of the cell suspension was then centrifuged onto poly-L-Lysine coated slides using a cytospin centrifuge. Cells were then fixed and stained as described below. For the repair kinetics experiments, cells were put on ice (for 10 min) at different time points post-irradiation. For repair times up to 1 h (2 min, 15 min, 30 min, 1 h) 0.5 ml of the cell suspension was centrifuged onto poly-L-Lysine coated slides. For longer incubation times (2 h, 3 h, 4 h, 5 h, 24 h), cells were transferred immediately after irradiation onto poly-L-Lysine precoated coverslips (20 × 20 mm, 50 μg/ml) in 6 well-plates and further incubated in serum starvation medium before being stopped on ice.

Immunocytochemistry

Cells were fixed with 3% paraformaldehyde (15 min for dose response experiments, overnight for repair kinetics experiments) and washed with Dulbecco's PBS (D-PBS) for 5 min. Cells were permeabilized in ice-cold D-PBS containing 0.2% Triton X-100 for 10 min and blocked in D-PBS containing 1% BSA (3 times for 10 min). Cells were incubated with anti-γ-H2AX antibody (1:500 in blocking buffer) for 1 h. After washing in blocking buffer (3 times for 10 min), cells were incubated with RAM-TRITC (1:1000 in blocking buffer) for 1 h. After rinsing in D-PBS, cells were mounted in slow-fade Gel Mount™ Aqueous Mounting Medium containing 2% 4',6-diamidino-2-phenylindole (DAPI) to counterstain the nuclei.

Automated slide scanning and detection of foci

For automated slide scanning and foci scoring, the Metacyte software module of the Metafer 4 scanning system (MetaSystems, Altlussheim, Germany) was used. The Metacyte operating mode offers the opportunity to scan slides for interphase nuclei in combination with spot detection and counting. In this mode, automated image acquisition is completed in two subsequent steps: first, the DAPI images are captured using a well defined cell selection classifier. This classifier consists of a group of parameters that precisely define the nuclear shape, size, etc. In a second step, the fluorescence filter is changed and the TRITC signals are captured in the selected nuclei. The acquired images are simultaneously stored and displayed in the image gallery, which contains an overview of the selected nuclei presented as the combined DAPI-TRITC image (Fig. 1). All TRITC signals were acquired as a z-stack with a total of 10 focal planes and a step size of 0.35 μm between planes.

A. Automated scoring of foci

Simultaneously with signal detection, spot counting is automatically performed in the Metacyte operating mode. Analysis of spots is based on two different approaches. The first approach, which is referred to as the 'direct spot count', is simply based on counting the number of spots within the nucleus: every spot is thereby scored as a single focus and the area and/or thickness of the focus is not taken into consideration. However, with increasing radiation dose, foci tend to melt into larger and/or thicker spots, and therefore the 'direct spot count' will yield an underestimation of the actual foci number. To cope with this problem another set of features is applied that leads to the second way of foci scoring: the 'corrected foci count'. This method takes into consideration the 3D structure of the detected spots and should therefore result in a better estimation of the actual number of foci, when radiation dose increases. These results are stored together with the acquired nuclei images and are depicted for each nucleus separately in the image gallery. Convenient histograms further provide information on the

Fig. 1. Screen shot of a slide automatically scanned using the Metacyte operating module (Metasystems). The selected image in the image gallery (red square) is relocated in the image area (yellow square). The image gallery consists of small images of the cells detected, displayed as a combined DAPI-TRITC image. In the under left and right corner of each image the direct foci count and the corrected foci count respectively, are depicted. The distribution of both counting methods is represented in the two bar histograms. The upper histogram is related to the direct spot count, the lower histogram to the corrected foci count. By clicking on these two histograms, the histogram tab sheet provides a data summary which lists the mean, standard deviation, coefficient of variation, minimum, maximum and median values of the analyzed cells. The search window, scaled to full size, further displays the positions of the cells detected on the slide.

distribution, the mean number and *SD* of the number of foci scored for each cell (Fig. 1). For each experimental condition, a minimum of 250 and a maximum of 500 cells were scored with these two methods and foci number was expressed as mean number of foci/cell.

B. Manual scoring of foci

To validate the automated foci scoring, the combined images stored in the image gallery, were manually analyzed by 2 independent scorers. This visual analysis of the number of foci/cell was performed for the first 100 cells captured. Six slides containing cells exposed to different radiation doses (0, 0.5 and 1 Gy) for both cell lines were taken into consideration. The mean number of foci/cell and its *SD* were then calculated and compared to the results obtained with full-automated scoring.

Statistical analysis

Statistical analysis of the data was performed using Statistical Package for Social Sciences (SPSS), version 15.0, software. For the validation of the automated scoring procedure Pearson's correlation coefficients (*r*s) were calculated. For the comparison of foci numbers in the two cell lines, independent sample t-tests were performed. For each of these tests, we report the appropriate values of *t*, the associated degrees of freedom and the level of statistical significance (*p*s).

RESULTS

Validation of automated foci scoring by image analysis

Validation of the automated foci scoring performed by the Metacyte spot counting software, was done by visual analysis of the first 100 images in the image gallery, by two independent scorers. These results were then compared with the equivalent automatic counts, which were based on the two different approaches: the 'direct spot count' and the 'corrected foci count' (Fig. 2). Analysis of different slides, representing different radiation doses (0, 0.5 and 1 Gy) for both cell lines revealed a good agreement between the manual counts of both scorers, all *r*s between .68 and .94, all *p*s < .01. Correlations between the observers' scores and the automated 'corrected foci count' ranged between .44 and .90, all *p*s < .01, indicating good agreement between the manual and the automated 'corrected foci count'. Figure 2 shows that both scorers and the automated corrected foci count yield very similar estimates of the number of foci, whereas the direct spot count yields a underestimation of this number in the irradiated samples. Because the corrected foci count allows for the separation of fused foci, this way of spot counting is expected to result in a better estimation of the actual number of radiation-induced foci.

Based on the good agreement obtained between the manual and automated corrected foci count of the same image sets, all the slides were further evaluated with this automated spot counting method. The automated processing of the slides offers both objectivity in scoring and increased statistical power by screening a large number of cells in a time-efficient manner.

Dose response experiments

Radiation-induced foci were calculated by subtracting the background number of foci in non-irradiated controls from the total number of foci scored in the irradiated samples. Foci formation was analyzed 15 min after exposure to γ-ray doses ranging from 0 to 4 Gy in the repair-deficient Ku70i and repair-proficient LVTHM MCF10A cells. Figure 3 shows that induction of γH2AX is dose dependent and a clear linear relationship between foci induction and dose is seen up to 1 Gy (Fig. 3B). At higher irradiation doses foci induction tends to reach a plateau. This is probably the result of the overlapping and melting of different foci into larger areas. Although the corrected foci count takes this phenomenon into consideration, it is no longer adequate for doses exceeding 2 Gy. Better results could be obtained by changing the features implemented to calculate the 'corrected foci count'. Separate independent samples t-tests on the average number of foci of two experiments at doses of 0.2, 0.5 and 1 Gy (see Fig. 3B) showed no difference between the two cell lines at 0.2 Gy and 0.5 Gy, $t(2) < 1$, $p = .51$, and $t(2) = 1.69$, $p = .23$, respectively. However, at a dose of 1 Gy, the number of foci in the Ku70i cell line was significantly higher than in the LVTHM cell line, $t(2) = 5.58$, $p < .05$. Further-

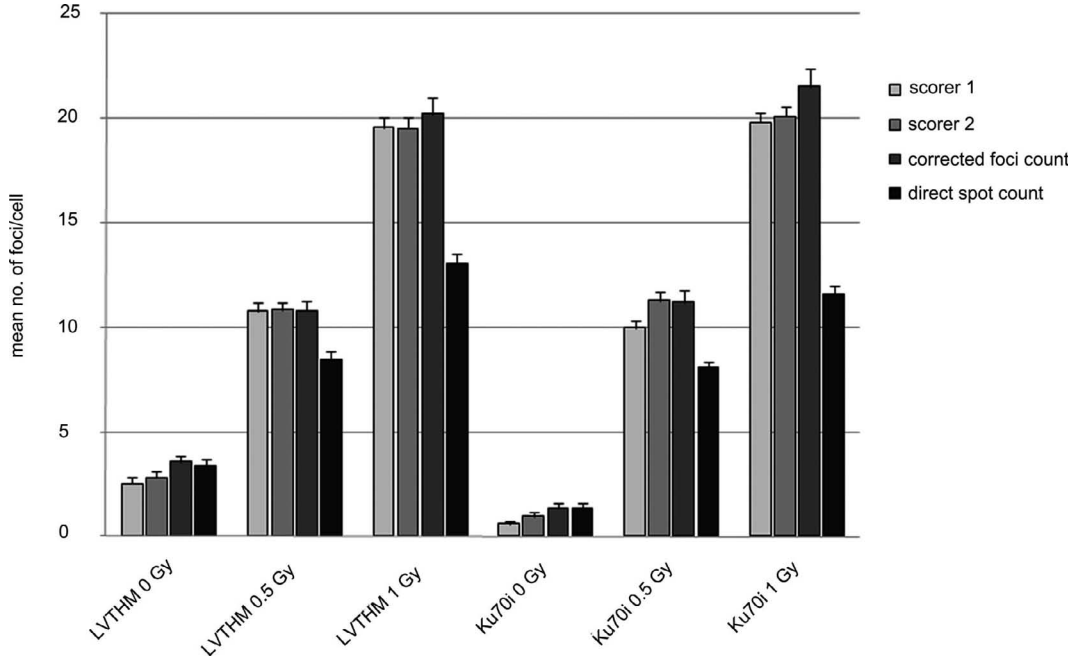

Fig. 2. Comparison between the number of foci obtained in the same cells by visual analysis by 2 scorers and automated analysis using 2 different approaches. For each data point 100 cells were analyzed. The figure depicts the mean number of foci/cell and the *SEM* (error bars).

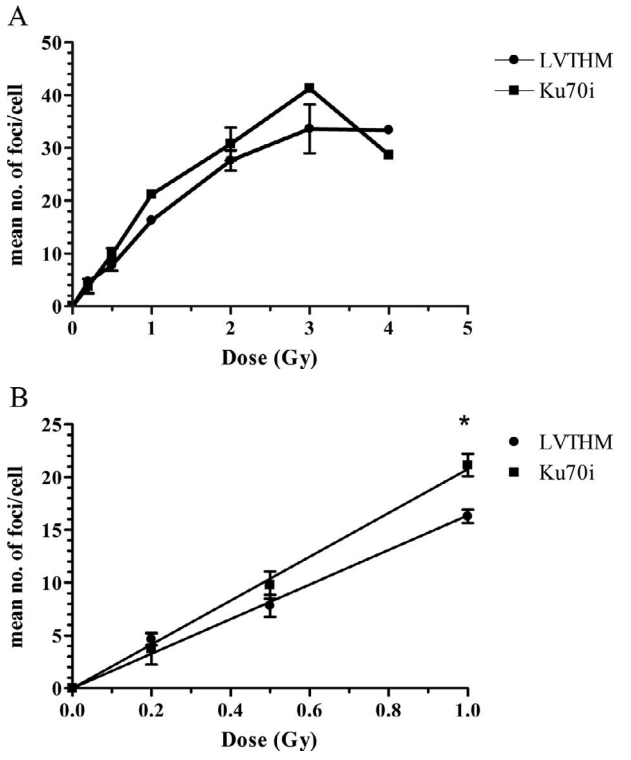

Fig. 3. Number of radiation-induced γH2AX foci/cell in G0/G1 synchronized Ku70i and LVTHM MCF10A cells as a function of radiation dose. Data points represent the mean of 2 independent experiments; error bars represent the *SD*. In Fig. 3B a linear curve was fitted through the data points. * $p < .05$.

more, this difference was significant within each experiment, $t(972) = 7.48$, $p < .001$, and $t(538) = 9.61$, $p < .001$.

Repair kinetics experiments

To study repair kinetics, induction and loss of γH2AX foci was investigated in the Ku70i and LVTHM cells at different time points after exposure to a γ-ray dose of 1 Gy. Figure 4 shows that the number of radiation-induced foci increased until 15 min after irradiation, reaching a maximum number of 13.06 (*SEM* = 0.93) foci/cell for the LVTHM and 15.39 (*SEM* = 0.54) foci/cell for the Ku70i cells. Then, the number of foci decreased gradually and parallel kinetics of γH2AX foci disappearance were observed. Separate independent samples t-tests on the average number of foci of three experiments at each of the nine time points (see Fig. 4) revealed marginally significant differences between the two cell lines at 15 minutes, $t(4) = 2.17$, $p = .096$, at 30 minutes, $t(4) = 2.25$, $p = .088$, and at 1 hour post-irradiation, $t(4) = 2.01$, $p = .11$. Importantly, these analyses may have lacked statistical power to reach significance. Therefore, we also conducted independent samples t-tests on the data of each individual experiment. These analyses showed that at 15 minutes post-irradiation, the number of foci/cell was in all three experiments significantly higher for the Ku70i cells: $t(641) = 6.99$, $p < .001$; $t(888) = 6.27$, $p < .001$; and $t(992) = 3.01$, $p < .005$. Similarly, in all three experiments, at 30 minutes post irradiation, more foci/cell remained in the Ku70i cells: $t(950) = 13.15$, $p < .001$; $t(971) = 6.29$, $p < .001$; and $t(963) = 5.27$, $p < .001$. Finally, in two of the three experiments at one hour post irradiation, the number of foci/cell in the Ku70i cells was significantly higher compared to the LVTHM cell line: $t(964) = 10.41$, $p < .001$; and $t(954) = 5.30$, $p < .001$. Hence, our data show that, at the early time points post-irradiation, the absolute number of radiation-induced γH2AX foci was higher in the Ku70i cells. At 24 h post-irradiation, radiation-induced foci levels in both cell lines returned to background levels ($M = 1.62$, $SD = 0.76$ for LVTHM cells and $M = 1.56$, $SD = 0.63$ for Ku70i cells), indicating the absence of any residual foci.

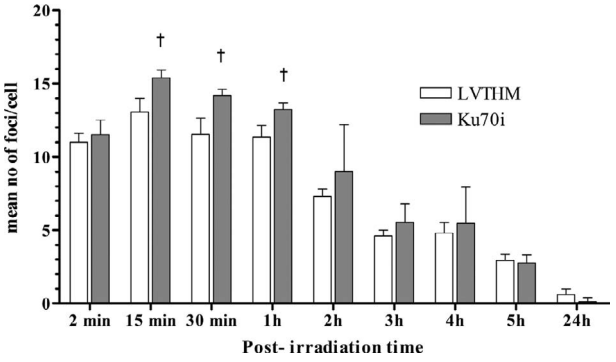

Fig. 4. Kinetics of radiation-induced γH2AX foci formation and loss in G0/G1 synchronized LVTHM and Ku70i MCF10A cells after irradiation with a γ-ray dose of 1 Gy. Data points represent the mean and error bars the *SEM* of 3 independent experiments. † $p < .11$.

DISCUSSION

In this study, we investigated whether the repair-deficient Ku70i cell line, previously characterized by an increased chromosomal and cellular radiosensitivity,[14] also shows differences in the phosphorylation pattern of the H2AX protein compared to the repair-proficient LVTHM cell line. If so, the γH2AX assay could prove to be a useful tool for the assessment of radiation sensitivity. All our results are based on automated scoring of foci number using Metacyte software. Preliminary validation of this automated system by comparison with manual foci analysis demonstrated the suitability of the automated scoring mode.

Our results show that compared to the repair-proficient LVTHM cell line, the repair-deficient Ku70i cell line has a significantly higher number of foci up to 1 h post-irradiation. After longer repair times, foci numbers decrease to similar levels in both cell lines and reach background levels after 24 hours.

Cell line dependent differences in the initial number of

γH2AX foci formation after irradiation have already been described.[39,41] In some cases these differences could be explained by the presence of different amounts of the H2AX protein between different cell lines. In mammalian tissues the amount of H2AX can vary between 2 and 25% of the histone H2A.[22] However, this explanation is unlikely to apply to our data since the LVTHM and Ku70i cell line are derived from the same wild type MCF10A cell line and by this have the same nuclear structure. Therefore, it can be assumed that the same amount of H2AX is present in both cell lines. Another possible explanation for the cell line dependent differences in initial foci formation is related to differences in kinase activity. ATM and DNA PKcs, both members of the PIKK family, have been argued to be the kinases that are involved in the phosphorylation of H2AX in response to radiation-induced DNA DSBs.[25] Since DNA PKcs is dependent on recruitment by the Ku heterodimer,[48] which binds directly to the ends of the DSB,[49] lower levels of Ku could result in less efficient recruitment of DNA PKcs. However, some evidence suggests that ATM and DNA PKcs function redundantly in the phosphorylation of H2AX in response to radiation-induced DSBs.[25] Moreover, ATM has been reported to play a dominant role in this phosphorylation event, while the contribution of DNA PKcs is rather limited[25] (for a review, see Stucki *et al*.[30]). Therefore, the reduced levels of Ku70 and Ku80 probably do not influence the H2AX phosphorylation process. Nevertheless, the lower levels of Ku proteins in the Ku70i cell line could compromise the 'fast' repair of simple DSBs. The group of Iliakis[35–38] indeed showed that in cells with mutations in DNA PKcs, Ku, DNA ligase IV or XRCC4, the fast component of NHEJ, operating with half times of 10–30 min, is strongly compromised. Since free DNA ends may not be captured directly or efficiently by the Ku proteins, a larger fraction of DNA DSBs will remain open and unrepaired for a longer duration compared to cells having wild type levels of the Ku proteins. Consistent with the idea that the loss of γH2AX only occurs after the break is rejoined, foci may be visible as long as the DNA ends are not rejoined and hence chromatin structure and integrity is not restored. Therefore, the presence of more foci at each time point up to 1 h may reflect a larger fraction of unrepaired DSBs and therefore slower kinetics of DSB repair in the early post-irradiation phase. Slower kinetics of DNA DSB repair have been further associated with an increase in misrejoining events as there is more time for exchanges between the free DNA ends.[35,37,50] Rejoining of incorrect ends leads to the formation of chromosome aberrations and this can be linked to the manifestation of a radiosensitive phenotype as was observed in our previous paper.[14]

Finally, although a number of studies reported a correlation between the presence of residual foci at longer repair times after radiation treatment and cellular radiosensitivity, we failed to detect any residual foci in both cell lines. These results are in line with those of Leatherbarrow *et al*.[33] also showing no residual foci in the radiosensitive Ku defective *xrs*-5 rodent cell line 24 h post-irradiation. To date, knowledge on the mechanisms and/or signals responsible for triggering the dephosphorylation of γH2AX foci is limited. If the physical sealing of the break, regardless of correct or incorrect rejoining, is associated with the disappearance of foci, unrejoined breaks could still manifest as visible γH2AX foci, while misrejoining events would not be detected by means of scoring residual foci at long times post-irradiation. However, the assumption has been made that residual γH2AX foci are not necessarily associated with unrejoined DSBs, which further demonstrates the lack of information regarding the nature of the residual foci.[39]

In summary, despite the significant higher amount of γH2AX foci at early post-irradiation times in the more radiosensitive Ku70i cell line compared to the LVTHM cell line, disappearance of those differences at later post-irradiation times questions the applicability of this assay to determine intrinsic radiosensitivity, especially in a clinical setting.

ACKNOWLEDGEMENTS

The work was supported by a grant of the 'Bijzonder Onderzoeksfonds' (Ghent University, No 01D30105), by a grant of the Research Foundation Flanders (FWO, No 1.5.080.08) and by a 'VLIR Own Initiative Programme' between Belgium and South Africa (ZEIN2005PR309).

REFERENCES

1. Kanaar R, Hoeijmakers JHJ and Van Gent DC (1998) Molecular mechanisms of DNA double-strand break repair. Cell Biol **8**: 483–489.
2. Khanna KK and Jackson SP (2001) DNA double-strand breaks: signaling, repair and the cancer connection. Nat Genet **27**: 247–254.
3. Mahaney BL, Meek K and Lees-Miller SP (2009) Repair of ionizing radiation-induced DNA double-strand breaks by non-homologous end-joining. Biochem J **417**: 639–650.
4. Weterings E and Chen D (2008) The endless tale of non-homologous end-joining. Cell Res **18**: 114–124.
5. Singleton BK, *et al* (1997) Molecular and biochemical characterization of xrs mutants defective in Ku80. Mol Cell Biol **7**: 1264–1273.
6. Ayene IS, Ford LP and Koch CJ (2005) Ku protein targeting by Ku70 small interfering RNA enhances human cancer cell response to topoisomerase II inhibitor and gamma radiation. Mol Cancer Ther **4**: 529–536.
7. Belenkov AI, *et al* (2002) An antisense oligonucleotide targeted to human Ku86 messenger RNA sensitizes M059K malignant glioma cells to ionizing radiation, bleomycin, and etoposide but not DNA cross-linking agents. Cancer Res **62**: 5888–5896.
8. Fattah KR, Ruis BL and Hendrickson EA (2008) Mutations to Ku reveal differences in human somatic cell lines. DNA Repair **7**: 762–774.

9. He F, *et al* (2007) Adenovirus-mediated expression of a dominant negative Ku70 fragment radiosensitizes human tumor cells under aerobic and hypoxic conditions. Cancer Res **67**: 634–642.
10. Li G, Nelsen C and Hendrickson EA (2002) Ku86 is essential in human somatic cells. Proc Natl Acad Sci USA **99**: 832–837.
11. Li GC, *et al* (2003) Adenovirus-mediated heat-activated antisense Ku70 expression radiosensitizes tumor cells in vitro and in vivo. Cancer Res **63**: 3268–3274.
12. Marangoni E, *et al* (2000) Transfer of Ku86 RNA antisense decreases the radioresistance of human fibroblasts. Cancer Gene Ther **7**: 339–346.
13. Omori S, *et al* (2002) Suppression of a DNA double-strand break repair gene, Ku70, increases radio- and chemosensitivity in a human lung carcinoma cell line. DNA Repair **1**: 299–310.
14. Vandersickel V, *et al* (2010) Lentivirus-mediated RNA interference of Ku70 to enhance radiosensitivity of human mammary epithelial cells. Int J Radiat Biol **86**: 114–124.
15. Kinner A, *et al* (2008) γ-H2AX in recognition and signaling of DNA double-strand breaks in the context of chromatin. Nucl Acids Res **36**: 5678–5694.
16. Takahashi A and Ohnishi T (2005) Does gammaH2AX foci formation depend on the presence of DNA double strand breaks? Cancer Lett **229**: 171–179.
17. Antoccia A, *et al* (2009) Cell cycle perturbations and genotoxic effects in human primary fibroblasts induced by low-energy protons and X/gamma-rays. J Radiat Res **50**: 457–468.
18. Hidaka M, *et al* (2010) Cell Lines Derived from a Medaka Radiation-Sensitive Mutant have Defects in DNA Double-Strand Break Responses. J Radiat Res **51**: 165–171.
19. Ishizaki K, *et al* (2004) No induction of p53 phosphorylation and few focus formation of phosphorylated H2AX suggest efficient repair of DNA damage during chronic low-dose-rate irradiation in human cells. J Radiat Res **45**: 521–525.
20. Kitajima S, *et al* (2010) AT Cells Show Dissimilar Hypersensitivity to Heavy-Ion and X-rays Irradiation. J Radiat Res **51**: 251–255.
21. Hansen JC (2002) Conformational dynamics of the chromatin fiber in solution: determinants, mechanisms, and functions. Annu Rev Biophys Biomol Struct **31**: 361–392.
22. Rogakou EP, *et al* (1998) DNA double-stranded breaks induce histone H2AX phosphorylation on serine 139. J Biol Chem **273**: 5858–5868.
23. Rogakou EP, *et al* (1999) Megabase chromatin domains involved in DNA double-strand breaks in vivo. J Cell Biol **146**: 905–916.
24. Burma S, *et al* (2001) ATM phosphorylates histone H2AX in response to DNA double-strand breaks. J Biol Chem **276**: 42462–42467.
25. Stiff T, *et al* (2004) ATM and DNA-PK function redundantly to phosphorylate H2AX after exposure to ionizing radiation. Cancer Res **64**: 2390–2396.
26. Kouzarides T (2007) Chromatin modifications and their function. Cell **128**: 693–705.
27. Sedelnikova OA, *et al* (2002) Quantitative detection of (125)IdU-induced DNA double-strand breaks with gamma-H2AX antibody. Radiat Res **158**: 486–492.
28. Rothkamm K and Löbrich M (2003) Evidence for a lack of DNA double-strand break repair in human cells exposed to very low x-ray doses. Proc Natl Acad Sci USA **100**: 5057–5062.
29. Redon C, *et al* (2002) Histone H2A variants H2AX and H2AZ. Curr Opin Genet Dev **12**: 162–169.
30. Stucki M and Jackson SP (2006) gammaH2AX and MDC1: anchoring the DNA-damage-response machinery to broken chromosomes. DNA Repair (Amst) **5**: 534–543.
31. Foster ER and Downs JA (2005) Histone H2A phosphorylation in DNA double-strand break repair. FEBS J **272**: 3231–3240.
32. Pilch DR, *et al* (2003) Characteristics of gamma-H2AX foci at DNA double-strand breaks sites. Biochem Cell Biol **81**: 123–129.
33. Leatherbarrow EL, *et al* (2006) Induction and quantification of gamma-H2AX foci following low and high LET-irradiation. Int J Radiat Biol **82**: 111–118.
34. DiBiase SJ, *et al* (2000) DNA-dependent protein kinase stimulates an independently active, nonhomologous, end-joining apparatus. Cancer Res **60**: 1245–1253.
35. Iliakis G, *et al* (2004) Mechanisms of DNA double strand break repair and chromosome aberration formation. Cytogenet Genome Res **104**: 14–20.
36. Iliakis G (2009) Backup pathways of NHEJ in cells of higher eukaryotes: cell cycle dependence. Radiother Oncol **92**: 310–315.
37. Wang H, *et al* (2003) Biochemical evidence for Ku-independent backup pathways of NHEJ. Nucleic Acids Res **31**: 5377–5388.
38. Wang M, *et al* (2006) PARP-1 and Ku compete for repair of DNA double strand breaks by distinct NHEJ pathways. Nucleic Acids Res **34**: 6170–6182.
39. Banáth JP, Macphail SH and Olive PL (2004) Radiation sensitivity, H2AX phosphorylation, and kinetics of repair of DNA strand breaks in irradiated cervical cancer cell lines. Cancer Res **64**: 7144–7149.
40. Taneja N, *et al* (2004) Histone H2AX phosphorylation as a predictor of radiosensitivity and target for radiotherapy. J Biol Chem **279**: 2273–2280.
41. MacPhail SH, *et al* (2003) Expression of phosphorylated histone H2AX in cultured cell lines following exposure to X-rays. Int J Radiat Biol **79**: 351–358.
42. Mahrhofer H, *et al* (2006) Radiation induced DNA damage and damage repair in human tumor and fibroblast cell lines assessed by histone H2AX phosphorylation. Int J Radiat Oncol Biol Phys **64**: 573–580.
43. Olive PL and Banáth JP (2004) Phosphorylation of histone H2AX as a measure of radiosensitivity. Int J Radiat Oncol Biol Phys **58**: 331–335.
44. Yoshikawa T, *et al* (2009) Phosphorylated H2AX foci in tumor cells have no correlation with their radiation sensitivities. J Radiat Res **50**: 151–160.
45. Bouquet F, Muller C and Salles B (2006) The loss of gammaH2AX signal is a marker of DNA double strand breaks repair only at low levels of DNA damage. Cell Cycle **5**: 1116–1122.
46. Furuta T, *et al* (2003) Phosphorylation of histone H2AX and

activation of Mre11, Rad50, and Nbs1 in response to replication-dependent DNA double-strand breaks induced by mammalian DNA topoisomerase I cleavage complexes. J Biol Chem **278**: 20303–20312.
47. Chanoux RA, *et al* (2009) ATR and H2AX cooperate in maintaining genome stability under replication stress. J Biol Chem **284**: 5994–6003.
48. Dynan WS and Yoo S (1998) Interaction of Ku protein and DNA-dependent protein kinase catalytic subunit with nucleic acids. Nucleic Acids Res **26**: 1551–1559.
49. Downs JA and Jackson SP (2004) A means to a DNA end: the many roles of Ku. Nat Rev Mol Cell Biol **5**: 367–378.
50. Kühne M, *et al* (2004) A double-strand break repair defect in ATM-deficient cells contributes to radiosensitivity. Cancer Res **64**: 500–508.

Received on March 12, 2010
Revision received on May 2, 2010
Accepted on June 7, 2010